INTERNATIONAL JOURNAL OF HYDROGEN ENERGY XXX (XXXX) XXX

Available online at www.sciencedirect.com

ScienceDirect

journal homepage: www.elsevier.com/locate/he

Decarbonization synergies from joint planning of electricity and hydrogen production: A Texas case study

Espen Flo Bødal [a,*], *Dharik Mallapragada* [b], *Audun Botterud* [c], *Magnus Korpås* [a]

[a] Norwegian University of Science and Technology, Trondheim, Norway
[b] MIT Energy Initiative, Massachusetts Institute of Technology, Cambridge, MA, USA
[c] Laboratory for Information and Decision Systems, Massachusetts Institute of Technology, Cambridge, MA, USA

HIGHLIGHTS

- Flexibility from electrolytic H_2 production enables more renewable integration.
- Carbon capture occurs at lower CO_2 prices for production of H_2 than electricity.
- Electrolytic H_2 production is dominant for CO_2 prices of \$30–60/tonne or more.
- Increased H_2 demand favors natural gas based H_2.
- Emissions are less than 1.2 kg CO_2/kg H_2 for CO_2 prices of \$90/tonne or more.

ARTICLE INFO

Article history:
Received 20 July 2020
Received in revised form
8 September 2020
Accepted 16 September 2020
Available online xxx

Keywords:
Hydrogen
Electrolysis
Power system analysis
Renewable energy

ABSTRACT

Hydrogen (H_2) shows promise as an energy carrier in contributing to emissions reductions from sectors which have been difficult to decarbonize, like industry and transportation. At the same time, flexible H_2 production via electrolysis can also support cost-effective integration of high shares of variable renewable energy (VRE) in the power system. In this work, we develop a least-cost investment planning model to co-optimize investments in electricity and H_2 infrastructure to serve electricity and H_2 demands under various low-carbon scenarios. Applying the model to a case study of Texas in 2050, we find that H_2 is produced in approximately equal amounts from electricity and natural gas under the least-cost expansion plan with a CO_2 price of \$30–60/tonne. An increasing CO_2 price favors electrolysis, while increasing H_2 demand favors H_2 production from Steam Methane Reforming (SMR) of natural gas. H_2 production is found to be a cost effective solution to reduce emissions in the electric power system as it provides flexibility otherwise provided by natural gas power plants and enables high shares of VRE with less battery storage. Additionally, the availability of flexible electricity demand via electrolysis makes carbon capture and storage (CCS) deployment for SMR cost-effective at lower CO_2 prices (\$90/tonne CO_2) than for power generation (\$180/tonne CO_2). The total emissions attributable to H_2 production is found to be dependent on the H_2 demand. The marginal emissions from H_2 production increase with the H_2 demand for CO_2 prices less than \$90/tonne CO_2, due to shift in supply from electrolysis to SMR. For a CO_2 price of \$60/tonne we estimate the production weighted-average H_2 price to be between \$1.30–1.66/kg across three H_2 demand

* Corresponding author.
E-mail address: espen.bodal@ntnu.no (E.F. Bødal).
https://doi.org/10.1016/j.ijhydene.2020.09.127

scenarios. These findings indicate the importance of joint planning of electricity and H_2 infrastructure for cost-effective energy system decarbonization.

Nomenclature

Indices

i	Plant type
n, m	Nodes
t	Time step

Costs

C_i^{energy}	Storage energy cost [$/MWh] or [$/kg]
C^e	Emission cost [$/kg]
C_i^{fix}	Fixed cost [$/plant]
C_i^{inv}	Investment cost [$/plant]
C_i^{power}	Storage power cost [$/MW] or [$/(kg/h)]
C_i^{rat}	Rationing cost [$/MWh] or [$/kg]
C_i^{ret}	Retirement cost [$/plant]
C_i^{var}	Variable cost [$/MWh] or [$/kg]

Parameters

η_i	Charge/discharge efficiency for storage type i
γ_i	Emission rate [kg CO_2/MWh] or [kg CO_2/kg H_2]
A_i	Auxillary electricity [MWh/kg]
D_{tn}	Electricity or H_2 demand [MWh] or [kg]
E_i	Cost of CO_2-emissions [$/kg]
F_i	Conversion rate [MWh/kg H_2] or [kg H_2/MWh]
P_i	Max or min plant capacity [MW] or [kg/h]
P_{tin}	Power profile [MWh]
R_i	Maximum ramping [MW] or [kg/h]
$T_{nm}^{init/max}$	Initial or maximum transmission capacity from node n to m [MW] or [kg/h]
$X_{in}^{init/max}$	Initial or maximum number of power plants

Sets

$\mathcal{L}$	Transmission lines and pipelines
$\mathcal{N}$	All nodes
$\mathcal{P}$	Plants types for electricity or H_2 production
$\mathcal{R}$	VRE power plants types
$\mathcal{S}$	Storage types
$\mathcal{T}$	Time steps

Indexed Sets

$\mathcal{A}_n$	Plants types requiring auxiliary power at node n
$\mathcal{B}_n$	Nodes connected to node n by transmission
$\mathcal{C}_n$	Nodes connected to node n by conversion plants
$\mathcal{F}_n$	Conversion plant types at node n
$\mathcal{P}_n$	Plants types at node n
$\mathcal{S}_n$	Storage types at node n

Investment Variables

e_n^{cap}	Storage charge/discharge capacity [MW] or [kg/h]
s_{in}^{cap}	Storage level capacity [MWh] or [kg]
x_{in}^{trans}	New lines or pipes
x_{in}	New plants

Operation Variables

c_{tin}	Energy curtailment of VRE [MWh]
$e_{tin}^{in/out}$	Storage charge/discharge [MW] or [*kg/h*]
f_{tnm}	Flow on lines or pipelines [MW] or [kg/h]
$p_{tn}^{exp/imp}$	Import/export [MW]
p_{tin}	Production [MW] or [kg/h]
r_{tn}	Load curtailment [MW] or [kg]
s_{tn}	Storage level [MWh] or [kg]
u_{tin}	Number of committed plants

Introduction

Policymakers across the world are looking for cost-effective ways to reduce CO_2 emissions by mid-century throughout all sectors of the economy to address climate change. Electrification of various end-uses is gaining traction as a cost-effective strategy for reducing CO_2 emissions in various sectors, most notably, light duty vehicle transportation [1]. Electrification not only improves end-use energy efficiency in many cases, but also concentrates emissions sources upstream, in the power sector, where decarbonization efforts are accelerating with the adoption of variable renewable energy (VRE) generation capacity. While direct electrification is appealing, it may be impractical in several end-uses such as industrial applications using fossil-fuel as feedstocks and heavy-duty transportation [2–4], where volumetric and gravimetric energy density are key performance requirements. In this context, use of alternative energy carriers like hydrogen (H_2) produced from electricity or other low-carbon sources remains an appealing prospect. Furthermore, H_2 can be used to produce ammonia and synthetic fuels that are well suited for directly replacing fossil based fuels, for example in shipping and aviation, without major modifications to existing machines or fueling systems [5–7].

The production of H_2 in the world today is almost entirely based on fossil energy sources, of which 76% is from natural gas and 23% from coal, with electrolysis accounting for less than 0.1% of supply [8]. To date, the relatively high cost of electrolytic H_2, estimated to be $4.8/kg using US costs, compared to fossil-fuel routes using natural gas ($1.2/kg) has limited its adoption [9]. Moreover, the cost of electrolytic H_2 production is dominated by the cost of electricity (~77% of total costs) when the electrolyzer is operated continuously [9]. Three factors are anticipated to change this picture. First, the investment costs of proton exchange membrane electrolysis (PEMEL) is projected to reduce substantially over the coming decades, with one estimate suggesting declines from $900/kW in 2018 to $400/kW by 2040 [10]. The future capital cost reduction for electrolytic H_2 will mainly arise from economies of scale and increased automation in the production of electrolyzers [11], but also larger electrolyzer stacks and multi-stack electrolysis plants [12]. Second, increasing penetration of VRE generation in the electric grid is anticipated to lead to more hours of zero wholesale electricity prices. Operating electrolyzers in a flexible manner can exploit these hours of low electricity prices for H_2 production while also providing demand-side flexibility to support greater levels of VRE integration in the electric grid [13–18]. Third, increasing policy emphasis on CO_2 emissions reduction is likely to favor H_2 produced from VRE electricity sources rather than fossil-fuel intensive H_2 production processes. Collectively, these factors raise the prospect of H_2 produced from electricity becoming competitive with natural gas based H_2 within the coming decades [12,19,20].

Unlocking cost-effective electrolytic H_2 production at scale could accelerate decarbonization of energy uses which are difficult to electrify, but can also provide large amounts of flexibility to the power grid when operated as a flexible load. Over-sizing the electrolyzer compared to the H_2 demand and installing H_2 storage enables the H_2 production to be flexible and produce more H_2 when there is a surplus of electricity (indicated by low prices) in the system and less when there is a deficit (indicated by high prices) [21–23]. In power systems with large shares of VRE generation, the variations in electricity price is expected to be higher than in current grids, implying that flexible H_2 production can significantly lower the electricity related H_2 production costs and increase plant profitability [24] compared to producing H_2 at a constant rate [20,22,25–27]. Furthermore, flexible electrolytic H_2 production is well suited to provide ancillary services to the electricity system, which can be an additional potential source of income for electrolyzers and contribute to reducing H_2 costs [28–31].

To accurately capture the value of flexibility from H_2 production by electrolysis, and thus the cost of H_2, it is necessary to model the operation of the electrolysis plant in conjunction with the electric power system directly. Furthermore, for a holistic estimate of the benefits provided by energy storage, either as H_2 or other storage types, it is important to consider an investment planning framework, as most of the benefits of energy storage or demand flexibility generally arise from deferring investments in new generation and transmission capacity [32,33].

Prior studies on the interactions between electricity and H_2 infrastructure, including production, storage and transport can be grouped according to the resolution used in the representation of various stages of the H_2 supply chain. Traditional electricity focused capacity expansion models include H_2 in the form of energy storage only, where a storage system is designed by combining electrolyzer, H_2 storage tanks and re-conversion by fuel cell or H_2 turbines [34,35]. This use of H_2 for electricity storage suffer from low round-trip efficiency, typically 30–50% [16], and is mostly used as a long-term storage option to complement other short-duration storage technologies.

Studies which focus on the H_2 supply chain, such as storage and transport in the form of pipes, compressed H_2 or liquefied H_2 trucks tend to have a simplified representation of the interactions with the electricity system such as residual loads or only VRE electricity supply [36–39].

Recently, a few studies have evaluated the flexibility provided by sector-coupling through coordinated expansion of electricity and H_2 infrastructure [40]. Some of these studies consider the use of H_2 for electricity storage [41] or as a complete system with H_2 demand. In general, the models with comprehensive H_2 system models often have restriction in term of spacial or temporal resolution [42,43] or are split into soft-linked investment and operation models [44], all of which impacts the results especially in VRE dominated systems. Models that include detailed electricity and H_2 system models usually only consider H_2 production by electrolysis and do not include H_2 produced from the dominant natural gas pathways [45]. Models that include H_2 production from natural gas tend to have a low spatial resolution [46] or low modeling detail of conventional electricity generation [47,48].

In this work, we develop a capacity expansion model to evaluate the cost-optimal electricity and H_2 infrastructure needed to serve future electricity and H_2 demand across a range of policy and technology scenarios. The modeling framework optimizes for investment subject to a number of operational and policy constraints. These include investment limitations on physical installations according to resource potential as well as operational limitations on generation and transport. Ramping constraints enforce the rate of change in electricity and H_2 production for the different technologies. Balance constraints keeps track of the balance between production and consumption, storage level and flow of H_2 and electricity between locations. The operational constraints are enforced while modeling hourly resolution of system operation throughout the entire year. We model electricity and H_2 transmission by overhead lines and pipelines respectively, as the best VRE sources often are located far away from major energy demand centers. H_2 is produced from PEMEL or natural gas with or without carbon capture and storage (CCS) and can be converted to electricity by a proton exchange membrane fuel cell (PEMFC) or H_2 compatible gas turbines. We model H_2 production from natural gas via steam-methane reforming (SMR). The model is applied for a case study of Texas in 2050 under a range of H_2 demand and carbon price scenarios. We summarize the new contributions to the literature arising from this work as follows:

a) We develop a coordinated electricity and H_2 system capacity expansion model with high temporal and spatial resolution that considers the dynamics between electricity and H_2 in terms of major technological options for production, storage and transport.
b) We conduct a comprehensive case study of electricity and H_2 production for the U.S. state of Texas with realistic assumptions, considering the impact of different CO_2 prices and H_2 demands.
c) The results show that flexible H_2 supply from PEMEL enables more integration of VRE and reduces battery storage

requirements in the grid. Moreover, increasing H_2 demand makes PEMEL more expensive, thereby shifting H_2 production towards SMR. Due to the synergies between VRE generation and PEMEL loads, we find that CCS adoption is attractive for SMR at lower CO_2 prices compared to CCS adoption for electricity generation in the power sector.

The rest of the paper has the following structure. In Section Method we describe the optimization model used for studying the interaction between H_2 and electricity infrastructure. Section Case study and input assumptions presents the electricity and H_2 system in Texas, as well as the baseline technical and economic assumptions to characterize electricity and H_2 demand, production, transport and storage technologies. Section Results discusses the model results under various CO_2 prices, technology costs and demand scenarios. Section Discussion and conclusion discusses the major findings of the work and identifies areas for future analysis.

Method

The joint electric and H_2 capacity expansion model finds the least-cost portfolio to meet future electricity and H_2 demand in a region. The model is formulated as a linear programming (LP) problem, as stated in Eqs (1)–(13). The electricity and H_2 parts of the system are separated by dedicating nodes to each respective energy carrier. The electric nodes are connected to electricity generating technologies, battery storage, transmission lines and electric loads. The formulation at H_2 nodes are equivalent to the electricity nodes, H_2 is produced from SMR with or without (w/wo) CCS to meet H_2 demand, stored in storage tanks or transported on H_2 pipelines as illustrated in Fig. 1. A set of technologies that consist of PEMEL, fuel cells

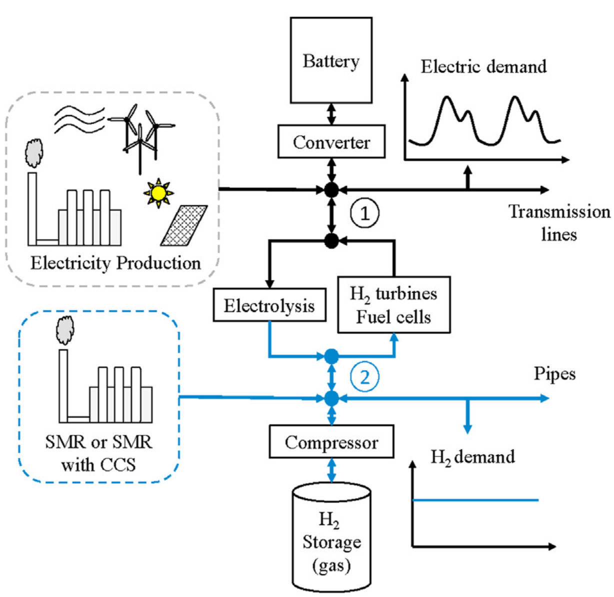

Fig. 1 – Schematic illustration of the energy balances in electric nodes (1) and a H_2 nodes (2). The system consist of several such node pairs connected by overhead lines and H_2 pipelines.

(PEMFC) and H_2 turbines are connecting the two types of nodes by representing generation on one side and loads on the other side. The technical features of electricity and H_2 technologies are described by the same set of constraints, which consist of operational limits on production and ramping determined by the commitment status and balances for energy, storage and transmission.

The objective function in Eq. (1) minimizes the investment, retirement, fixed and variable operational costs. The total investment cost is represented by the sum of all individual investments in electricity generating power plants, PEMEL, SMR w/wo CCS, power converters, pumps, batteries, H_2 tanks and transmission capacity in the form of overhead lines and pipelines. The investments in storage capacities are represented by separate power and energy capacities. Variable operational costs arise from fuel costs and variable O&M costs, in addition we consider a technology dependent emission rate and a uniform CO_2-emission cost. At a given time period, unserved electricity or H_2 demand is associated with a penalty.

$$\min \sum_{n\in\mathcal{N}} \Big[\sum_{i\in\mathcal{P}}(C_i^{inv}x_{in} + C_i^{ret}x_{in}^{ret} + C_i^{fix}(X_{in}^{init} + x_{in} - x_{in}^{ret})) + \sum_{i\in\mathcal{S}}(C_i^{power}e_{in}^{cap} + C_i^{energy}s_{in}^{cap}) + \sum_{n,m\in\mathcal{L}} C_{nm}^{Trans}x_{nm}^{trans} + \sum_{t\in\mathcal{T}}\Big[\sum_{i\in\mathcal{P}}(C_i^{var} + \gamma_i C^e)p_{tin} + \sum_{n\in\mathcal{N}} + C^{rat}r_{tn}\Big]\Big] \quad (1)$$

Power plants and H_2 production facilities are grouped by technology and location. This allows us to model commitment and expansion decisions as integers instead of binaries, an approach that is shown to drastically reduce the computational time with low approximation errors [49]. We also relax the integer commitment and investment decision to be continuous in order to further reduce the computational time, which has been shown to be a reasonable approximation [50, p. 162–174] especially when the optimal integer variable is much greater than 1. Investments in new capacity is bounded by an upper limit that typically represents the resource potential at a given location, as stated in Eq. (2).

$$x_{in} \le X_{in}^{max} \quad \forall i\in\mathcal{P}, \forall n\in\mathcal{N} \quad (2)$$

The operation of the system is governed by Eqs 3–14 for all times, $\forall t\in\mathcal{T}$, and all nodes, $\forall n\in\mathcal{N}$. The plants that can be committed for operation is restricted by the investment decisions as stated in Eq. (3). The plants have both minimal and maximum production limits as shown in Eq. (4). They also have ramping constraints that limit how fast they can increase or decrease their production from one period to another as shown in Eq. (5). The relaxation of the commitment decisions allows power plants to ramp faster than what is technically possible. However, the combination of ramping and minimum production constraints gives a reasonable level of detail in the representation of power plant operations for this type of investment model.

$$u_{tin} \le X_{in}^{init} + x_{in} - x_{in}^{ret} \quad \forall i\in\mathcal{P} \quad (3)$$

$$P_i^{min}u_{tin} \le p_{tin} \le P_i^{max}u_{tin} \quad \forall i\in\mathcal{P} \quad (4)$$

$$-R_i u_{tin} \le p_{tin} - p_{(t-1)in} \le R_i u_{tin} \forall i \in \mathcal{P} \quad (5)$$

Available VRE production is used for producing electricity unless it is curtailed as stated in Eq. (6).

$$p_{tin} + c_{ti} = P_{tin}(X_{in}^{init} + x_i) \quad \forall i \in \mathcal{R} \quad (6)$$

The energy balances for electricity and H_2 are represented by the same constraint as stated in Eq. (7). Electricity or H_2 is produced or imported to serve the demand or export. Indexed sets determines the generation, storage and conversion technologies at each specific node. $\mathcal{P}_n$ represents the different generating technologies, i.e. power plants at the electric nodes or PEMEL and SMR at the H_2 nodes. H_2 and electricity can be shifted in time by using storage to add or withdraw from the energy balances. Unserved demand is penalized in the objective function. The set of conversion technologies, $\mathcal{F}_n$, are defined at the node they are producing. Conversion technologies used to produce H_2 or electricity at node n represents a load at a node of the opposite type specified by $\mathcal{C}_n$. Similarly, auxiliary electricity for H_2 compression is represented as an additional load. An illustrative example of the energy balance is given in Appendix A.

$$\sum_{i \in \mathcal{P}_n} p_{tin} - p_{tn}^{exp} + p_{tn}^{imp} + \sum_{i \in \mathcal{S}_n} (e_{tin}^{out} - e_{tin}^{in}) + r_{tn}$$

$$= D_{tn} + \sum_{m \in \mathcal{C}_n} \left(\sum_{i \in \mathcal{F}_m} F_i p_{tim} + \sum_{i \in \mathcal{A}_m} A_i e_{tim}^{in} \right) \quad (7)$$

The storage balance for the two different storage types batteries and H_2 storage, specified by index i, is shown in Eq. (8). The storage balance states that the electricity or H_2 stored is given by the energy stored in the previous time-stage plus the net energy input into the storage. The maximum storage level is restricted by the storage level capacity in Eq. (9). The rate in which the storage can be loaded or unloaded is given by in Eqs (10) and (11), which corresponds to the installed converter or compressor capacity.

$$s_{tin} = s_{(t-1)in} + \eta^{in} e_{tin}^{in} - (1/\eta^{out}) e_{tin}^{out} \quad \forall i \in \mathcal{S} \quad (8)$$

$$s_{tin} \le s_{in}^{cap} \quad \forall i \in \mathcal{S} \quad (9)$$

$$e_{tin}^{out} \le e_{in}^{cap} \quad \forall i \in \mathcal{S} \quad (10)$$

$$e_{tin}^{in} \le e_{in}^{cap} \quad \forall i \in \mathcal{S} \quad (11)$$

Power exchange between electric nodes or H_2 flow between H_2 nodes are governed by Eq. (12). The exchange balance states that the net electricity or H_2 exchanged with the rest of the system is equal to the flows in all the pipelines or overhead lines which are connected to the node. The maximum flow in the individual pipelines or overhead lines are bound by their respective capacity in Eqs (13) and (14). We simplify the physical electricity and H_2 flow and use a transport model as the individual lines and pipes are aggregated into transmission corridors. Thus, electric transmission losses and hydrogen compression for pipeline transport are not taken into account. Line-packing for the hydrogen pipelines represents a potential way of storing hydrogen in the pipelines, but is not considered in this model.

$$p_{tn}^{exp} - p_{tn}^{imp} = \sum_{m \in \mathcal{B}_n} f_{tnm} \quad \forall n \in \mathcal{N} \quad (12)$$

$$f_{tnm} \le T_{nm}^{init} + T_{nm}^{max} x_{nm}^{trans} \quad \forall n, m \in \mathcal{L} \quad (13)$$

$$f_{tnm} \ge -(T_{nm}^{init} + T_{nm}^{max} x_{nm}^{trans}) \quad \forall n, m \in \mathcal{L} \quad (14)$$

The model is implemented in the Python programming language, using the Pyomo modeling framework for optimization models [51,52] and solved by the Gurobi solver.

Case study and input assumptions

We assess the configuration of a joint H_2 and electricity system to supply future electricity and H_2 demand for the state of Texas in 2050. Texas represents an interesting case study, since: a) it is a region with high quality VRE resources, which has been noted as the state with the highest H_2 production potential from wind and solar power in the US [13], b) cheap availability of natural gas based on close proximity of natural gas resources, and c) significant existing H_2 demand from various petrochemical operations.

The electricity system in Texas, regulated by the Electric Reliability Council of Texas (ERCOT), is currently dominated by fossil energy sources, i.e. mainly natural gas but also coal. However, the north-western and western parts of Texas have excellent wind and solar resources. Although these are located far away from the major load centers in the east and south-east it is one of the fastest growing renewable regions in the world [53]. H_2 can be produced at the energy source and then transported to the consumers via pipelines. Alternatively the energy can be transported by electric transmission lines and used for H_2 production close to the point of consumption. We use a 13-node model of the Texas power system as shown in Fig. 2 [54], which indicate the spatial distribution of nodes where production and consumption of electricity and H_2 is located and possible pathways for new overhead lines and pipelines. We initialize the model with existing generation

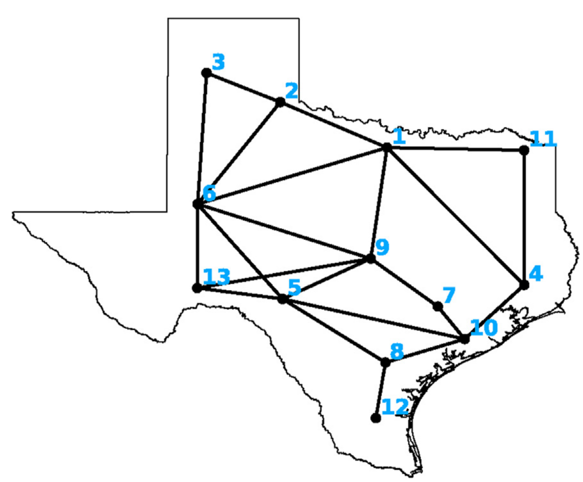

Fig. 2 – The spacial representation and distribution of nodes and the pathways considered for the overhead lines/pipelines in the Texas case study.

capacity at each node as of 2018 sourced from the NEEDS database [55] (see Table B 2).

Electricity and H_2 demand

The baseline electricity demand for 2050 is calculated based on an average yearly growth of 1% [56] from 2015. The annual electric load from the region is increased from 347 TW h in 2015 to 492 TW h in 2050, a relative increase of 42%. The load profile is obtained by using the actual loads in 2015 from the eight different weather zones defined by ERCOT [57]. The load profiles are transformed to node level by distributing the loads from zone to county level based on population distribution across counties and then aggregating the county-level load to the closest node.

As compared to electricity demand, there is substantial uncertainty in the demand for H_2 in 2050 given its relatively narrow use in industrial processes today. For this study, we defined a baseline scenario of H_2 demand based on a projection from NREL regarding potential H_2 use in the transportation sector by 2050 [58]. While this demand estimate is based on the transport sector, from the model perspective, the demand could also be viewed to represent H_2 consumption in other sectors as well. For simplicity, we have assumed a constant temporal profile for H_2 consumption throughout every hour of the year, with daily consumption estimates reported in the Appendix (Table B.6). Furthermore, we exclude the existing H_2 demand from industrial operations in Texas, since many of those facilities are served by on-site H_2 supply.

The annual baseline H_2 demand in this analysis is 0.68 million metric tonnes (mmt)/year. For reference, this is around 17% of the potential H_2 demand in the Texas "triangle" region at 3.9 mm t/year based on 2015 gasoline consumption [59]. Currently, the total US H_2 demand is around 10 mm t/year [60] and preliminary analysis in the H_2@Scale project estimates potential hydrogen demand in 2050 to be more than 9 times current levels (~ 100 mm t/year) [61]. Although a detailed analysis of potential H_2 demand is outside the scope of this work, we do consider the impact of scaling the baseline H_2 demand by a factor of 10 and 50.

H_2 production

Today, large scale H_2 production is mainly based on SMR and is associated with life cycle greenhouse gas (GHG) emissions of 10–16 kg CO_2eq/kg H_2 [62–64], of which process emissions account for approximately 9 kg CO_2/kg H_2 [62]. The cost of H_2 production is dominated by fuel costs, with the cost of natural gas accounting for 72% of the levelized cost in the U.S. ($1.15–1.32/kg H_2 [9]). 90% of the operational CO_2-emissions from the SMR-process can be captured by including CCS, with an estimated cost of to be $47–110/tonne CO_2 captured (levelized cost of $0.3–2.1/kg H_2) [64]. For this study, we assume that CCS lowers the plant GHG emissions associated with H_2 production from natural gas down to 0.93 CO_2/kg H_2 at a cost of $83/tonne CO_2.

The plant design, capacity costs, variable costs, fixed costs and emissions used in this analysis is based on the techno-economic evaluation of merchant SMR H_2 plants by the IEA [64]. They give a detailed breakdown of costs for SMR with or without CCS for a plant with a capacity of 216 tonnes H_2/day. Natural gas prices and the cost for carbon transportation and storage are streamlined for both H_2 and electricity producing technologies and set to be $5.24/MMBtu [65] and $11/tonne CO_2 [66] respectively.

We model the cost and performance for PEMEL plants based on the H2A production studies available from NREL [9]. The plant cost and performance is based on 60 tonnes H_2/day, with an installed capital costs of ~ $530/kW, which is in line with the long-term cost projections for multi-MW electrolysis plants in the literature [8,10,20,67,68]. The energy requirement for H_2 compression to 100 bar for storage is modeled to be 1.3 kW h/kg [69], and related capital costs are estimated to be $1200/kW [67]. The electrolysis plant has a state-of-the-art efficiency of 65% based on LHV. Further details on costs and characteristics for the H_2 producing technologies are found in Table B 4.

H_2 storage in pressure vessels (100 bar) buried underground at 100 bar is estimated to cost $516/kg [70,71]. Geological H_2 storage in salt caverns are the most cost-effective method for storing large quantities of H_2 [72] and currently widely used for natural gas and H_2 storage in Texas [67,73]. However, availability of salt caverns storage capacity is uncertain and therefore is not included in this analysis.

Electricity generation and storage

Investment, fixed and variable operating & maintenance costs in 2050 for electricity generation technologies were sourced from the mid scenario of the NREL Annual Technology Baseline 2019 edition [65]. This includes the cost of battery storage, where we separately define the cost of power and energy and allow the model to figure out the optimal energy to power ratio (i.e. duration) to be deployed at each location. The cost for H_2 re-conversion technologies are obtained from Refs. [37], and includes H_2 compatible gas turbines and PEMFC. Further details are available in Table B 3.

Energy transport

The cost of overhead line transmission expansion is modeled using a cost per mile estimate of $3000/(miles•MW) for the first 5 GW and $4000/(miles•MW) for the next 5 GW of each transmission corridor. This estimate is based on the costs of the CREZ transmission expansion in Texas at $2500/(miles•MW) and set higher to account for lines in more urban areas and decreasing future land availability [74]. The system is updated to include the CREZ expansion of ~ 11.5 GW [75,76] and investments in new transmission capacity is limited on each segment to 15 GW. H_2 pipelines are set to have a investment cost of $210/(m•GW) and $560/m [36].

Computation

The computation time for the model ranges from 1 to 2 h for each set of parameters. The parameters are changed in an automatic loop to do sensitivity analysis on the CO_2 price, resulting in 10 iterations and a total of 16–18 h of computational time. The computations are performed on a shared server typically using 28 threads for the optimization and up to 50–60 GB of memory. The processor is an Intel Xeon E5-2690 v4 with a clock frequency of 2.6 GHz (28 cores and 56 logical processors).

Results

Implications of CO_2 price

To investigate the effects of a CO_2 price, we run the model for different CO_2 prices in increments of $30/tonne from 0 to 270 $/tonne. This range spans the range of social cost of carbon estimated for 2050 by the US Environmental Protection Agency (EPA), which results show CO_2 prices from $69/tonne to $212/tonne [77].

Fig. 4.1 shows that introducing a CO_2 price of $30/tonnes leads to a significant growth in VRE electricity from 58 to 78 GW for wind power and 39–53 GW for solar power. In fact, this CO_2 price is on par with the European CO_2 quota prices in most of 2019 and 2020 at $30–35/tonne. The initial growth in VRE is followed by a more gradual growth when the CO_2 price is increased further. The deployment of VRE is followed by a large deployment of battery storage from 3 to 23 GW

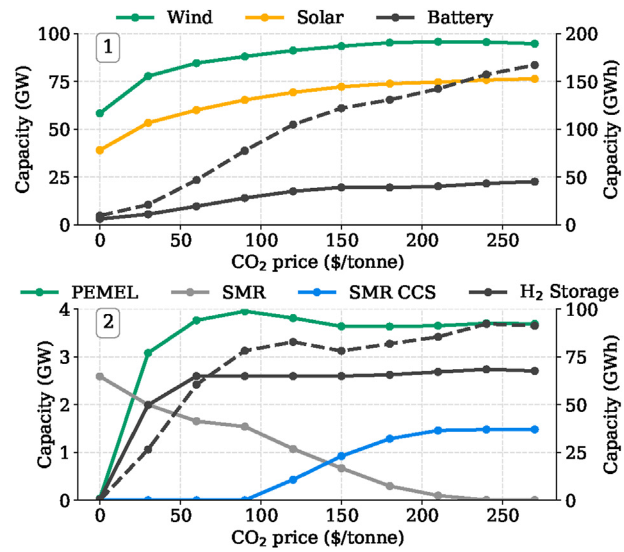

Fig. 4 – 1) VRE and battery capacity and 2) H_2 production and storage capacity as a function of the CO_2 price. H_2 capacities are converted to power by the lower heating value of H_2. Storage energy capacity is represented by the dotted lines and secondary y-axis (right).

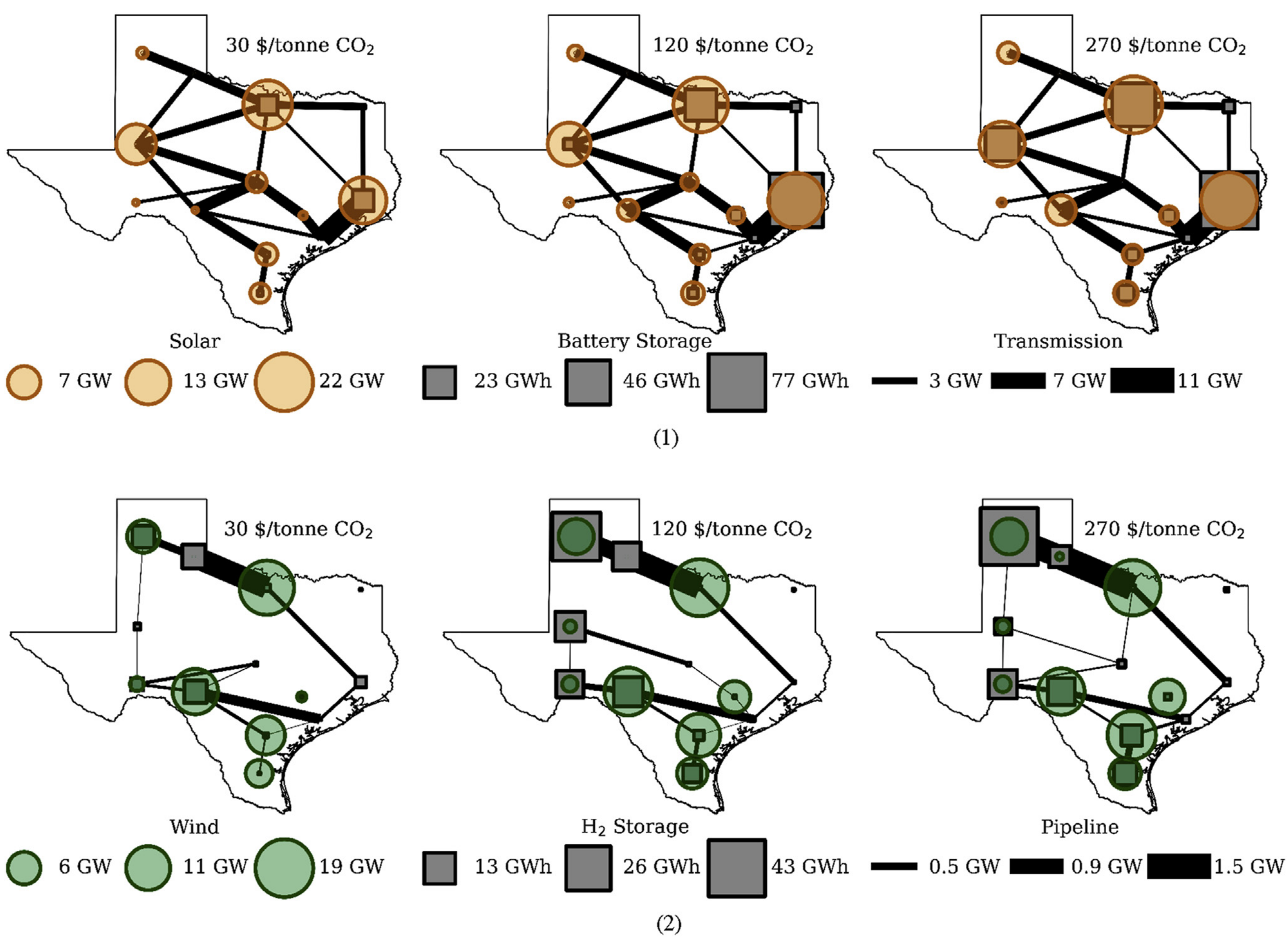

Fig. 3 – Development in 1) solar power, battery energy and overhead transmission line capacity and 2) wind power, H_2 storage and pipeline capacity. Overhead lines and pipelines with capacity under 1 GW and 1 tonne/h are excluded.

(10–167 GW h), where the storage duration (energy capacity divided by power capacity) increases linearly from 2 to 7 h.

H_2 is entirely produced from SMR in the absence of a price for CO_2 emissions as shown in Fig. 4.2. However, the H_2 share from SMR is gradually reduced with increasing CO_2 prices as SMR leads to significant emissions. Significant shares of the H_2 production is initially taken over by PEMEL with storage that can produce H_2 from electricity in surplus periods, followed by SMR with CCS for a CO_2 price higher than $90/tonne. H_2 capacities are converted to power by the lower heating value of H_2 ($LHVH_2$ = 33.3 kW h/kg), placing the largest amount of H_2 storage capacity at 12% and 54% of the maximum battery storage capacity for power and energy respectively, not accounting for efficiency of converting H_2 back to power. The duration of the H_2 storage increase from 13 to 36 h of H_2 supply when PEMEL capacity is built out (CO_2 prices of $30/tonne or more).

The spatial deployment of VRE generation, storage and transmission capacity is shown in Fig. 3 at CO_2 prices of 30, 120 and 270 $/tonne. At low CO_2 prices, solar power is primarily developed close to the main load centers in the east/north and in the west where solar irradiation is high, and is co-located with significant battery capacity as shown in Fig. 3.1. With increasing CO_2 prices and thus VRE deployment, more solar capacity is constructed in the south and west. The transmission capacity from west to east is also upgraded in the southern part of the state. Significant amounts of battery capacity is constructed in the nodes where solar power plants are located. Batteries appear to be preferred over new transmission capacity due to the intermittent VRE electricity production, and the limited geographical smoothing of solar PV output.

Wind power is initially developed in the south/south-west and north/north-west as shown in Fig. 3.2. H_2 storage supports the integration of wind and solar in western Texas and two main H_2 pipeline corridors are constructed going from west to east. For higher CO_2 prices more wind power is developed in the north-west, also called the Texas panhandle, and in the south. H_2 pipeline infrastructure connecting these two regions to the major demand regions in the west are reinforced. Most of the H_2 storage capacity is deployed at a CO_2 price of $120/tonne in contrast to the development in battery storage capacity that continues for higher CO_2 prices.

Solar power generation and battery storage charging has a correlation coefficient that is increasing with the CO_2 price, from around 0.28 to 0.45, which is higher than wind-battery and VRE-PEMEL correlations of 0.2–0.3. VRE-PEMEL correlation increase to the level of solar-battery correlation for higher H_2 demands, while wind-battery correlation stay low. This shows that batteries are synergistic with solar power development while flexible H_2 production is supporting the integration of both solar and wind power as shown in previous studies on H_2 production in the electricity system [35,41]. This is also supported by the resulting optimal duration of battery (2–7 h) and H_2 storage (5–36 h), and the locations for the different storage types observed in Fig. 3.

Effect of increasing the H_2 demand

The baseline H_2 demand assumed here is only a small fraction of the total electricity demand. To understand the implications of higher H_2 demand, we analyzed two additional scenarios for H_2 demand corresponding to 10X (scenario b) and 50X (scenario c) the baseline demand (scenario a). The additional H_2 demand can be interpreted to represent H_2 demand for industry, heavy-duty transportation or export of H_2 to other states or countries. For context, the H_2 demand in case a, b and c is equivalent to 4.6, 46 and 230% of the total electric demand in the system, respectively, if converted to energy by the LHV_{H_2} (assuming no losses).

The maximum VRE share is significantly increased from (a) 86.4% to (b) 90.9% and (c) 95.8% as shown in Fig. 5.1. In the scenarios with higher H_2 demand, (b) and (c), the capacity of battery storage required to integrate VRE generation is actually reduced as shown in Fig. 5.2. This is because the flexibility from producing large amounts of H_2 enables the integration of more VRE energy without requiring massive amounts of batteries or natural gas power plants. In (c), we get a VRE share as high as 94% at a CO_2 price of $60/tonne and 1.3 GW of battery storage, while the same CO_2 price gives a VRE share of 78% in scenario (a) and 87% in scenario (b) requiring 9.7 and 5.9 GW of battery storage respectively.

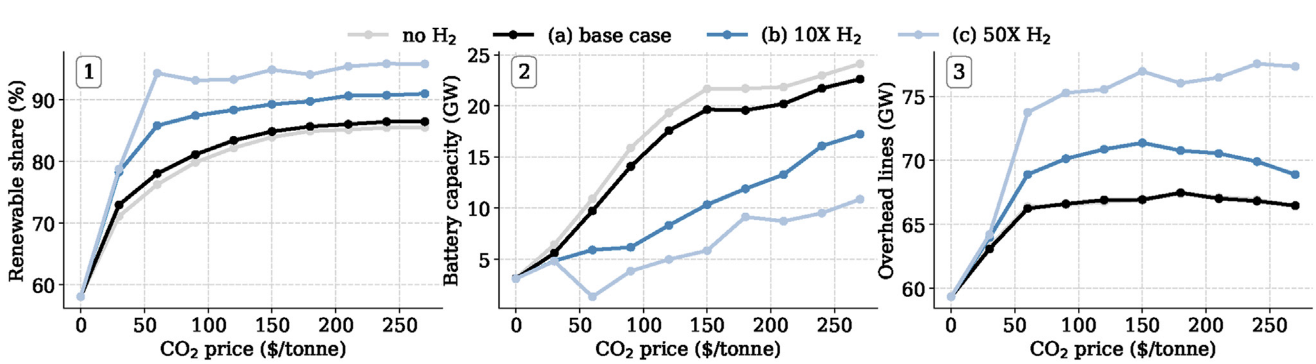

Fig. 5 – 1) VRE share of total electricity production, 2) battery storage capacity (power) and 3) transmission line capacity, by CO_2 price for the different H_2 demand scenarios.

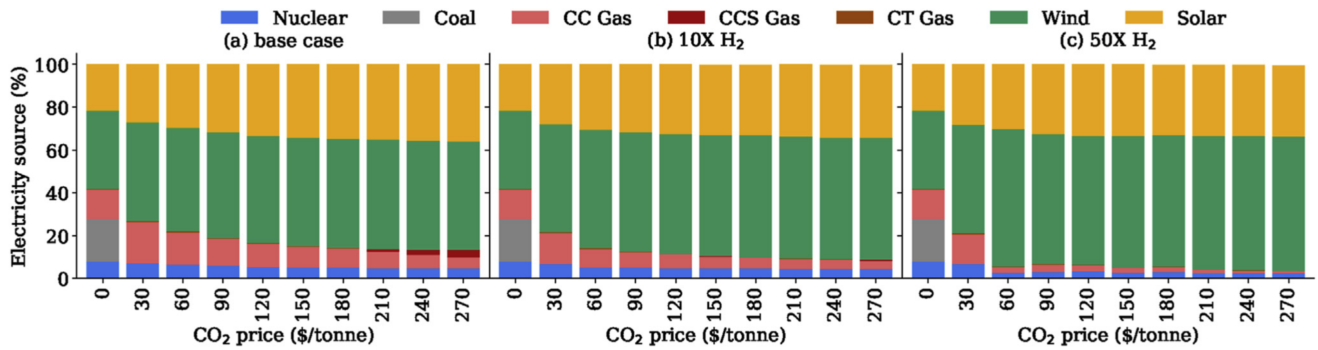

(1) Electricity produced by technology for the different CO_2 prices and H_2 demands.

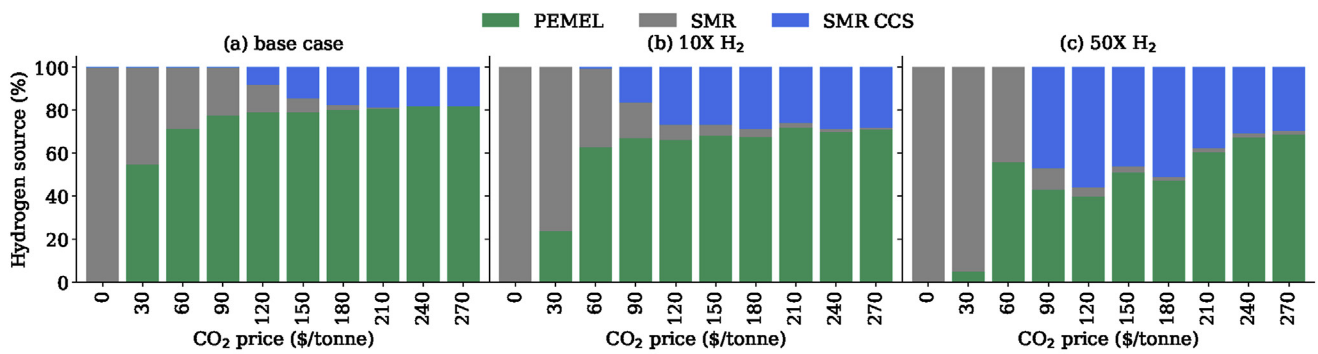

(2) Share of H_2 demand by production technology for the different H_2 demand scenarios.

Fig. 6 – Share of electricity and H_2 produced by the different technologies for different CO_2 prices and H_2 demand scenarios.

Integrating VRE requires significant transmission expansion as shown in Fig. 5.3, most of which is realized at a CO_2 price of $60/tonne. The availability of demand flexibility from sources such as electrolytic H_2 production also increases the impact of battery storage and transmission investments with increasing VRE penetration, as highlighted by the increase in VRE penetration with increasing H_2 demand seen in Fig. 5.1. Higher H_2 demand also contributes to reducing the levels of VRE curtailment (defined as percent of available VRE generation), which changes from (a) 6–13% to (b) 5–10% and (c) 4–20% for a CO_2 price above $30/tonne. Scenario (c) with high CO_2 prices results in a large amount of H_2 production from VRE and more than 500 GW of renewable capacity with a curtailment level of almost 20%. However, for a CO_2 price of $60/tonne the installed renewable capacity is 425 GW with significantly lower levels of curtailment at 13%.

The electric energy generation mix for different CO_2 prices and H_2 demands are shown in Fig. 6.1. The electricity produced from coal is reduced to zero at a CO_2 price of $30/tonne. Some of this energy is replaced by natural gas with lower emission intensity and higher operational flexibility than coal. Natural gas is gradually replaced by more VRE generation as demand side flexibility is provided by H_2 produced from PEMEL. Electricity generation from natural gas is reduced by up to (a) 5%, (b) 27% and (c) 53% for CO_2 prices of $30/tonne or higher compared to a reference case with no H_2 production.

Moreover, for CO_2 prices of $180/tonne and above we observe some of the natural gas being replaced by natural gas with CCS. The break-even CO_2 price for CCS adoption in the power sector is higher than those noted by other studies in the literature, primarily [78], because of the synergy between flexible demand from electrolytic H_2 and VRE generation. Gas based electricity generation has lower levelized cost of energy (LCOE) when CCS is included for CO_2 prices of $70/tonne or higher assuming a unity capacity factor (based on the input parameters). This threshold for CCS deployment increases to 100, 150 and 200 $/tonne CO_2 for lower capacity utilization of 0.5, 0.3 and 0.2 as lower utilization favors generation with lower capital expenses (without CCS). Fig. 6.1 shows that the break-even cost of natural gas with CCS is moved to higher CO_2 prices as the H_2 demand increase and more flexibility is available from the H_2 system. In general, the need for flexibility from natural gas based electricity generation is reduced with increasing H_2 demands, which leads to lower utilization of the gas power plants and less incentives to adopt the more capital intensive CCS options. H_2 for electricity generation requires CO_2 prices of more than $210/tonne for scenarios a and b, and $180/tonne for scenario c. Moreover, the share of H_2 to power generation in those cases is less than 0.5% of total generation (not visible in Fig. 6.1).

We compare the shares of the total H_2 demand obtained from the different H_2 plant types, PEMEL, SMR and SMR with CCS, in Fig. 6.2. H_2 is exclusively produced from SMR if no CO_2 pricing is in place. Increasing CO_2 prices favor H_2 production from PEMEL as compared to SMR. The lowest CO_2 price of $30/tonne results in a drastic increase in the H_2 produced from PEMEL to 55% of the total H_2 production in the base case. However, PEMEL becomes less competitive with SMR when producing larger quantities of H_2 as the electricity demand for PEMEL increases and there is a limited number of hours with VRE surplus and very low electricity prices. As a result, an increasing H_2 demand favors SMR and the PEMEL share at a CO_2 price of $30/tonne is reduced to 24% and only 5% of the H_2 produced in case (b) and (c) respectively.

A CO_2 price of $120/tonne is required to introduce CCS with SMR in the base case, as seen from Fig. 6.2. This is higher than the cost of CO_2 capture for SMR ($83/tonne) because of electrolyzer flexibility and synergy with VRE generation and less than 100% utilization of the SMR plant. Beyond $120/tonne, there is less incentive to shift to electrolytic H_2 supply because of the reduced marginal emissions penalty associated with natural gas based H_2 production with CCS. SMR with CCS is introduced for a lower CO_2 price ($90/tonne) in (b) and (c) as H_2 from PEMEL becomes less competitive with higher hydrogen demand and SMR capacity utilization increases. However, at the highest hydrogen demand in scenario (c) and high CO_2 prices (≥$180/tonne) hydrogen production shifts from SMR with CCS to PEMEL as the former represents a significant share of the total emissions. Here, the maximum electrolyzer capacities for Texas are (a) 6, (b) 47 and (c) 218 GW. As a point of comparison, the newly stated targets by the European Commission are at least 6 and 40 GW of electrolyzer capacity to be installed by 2024 and 2030 respectively [79].

Total and relative CO_2 emissions

Fig. 7 shows the total emissions from joint electricity and H_2 production for a range of CO_2 prices. For comparison between the scenarios, we define the base demand scenario without a CO_2 price as a reference, with emissions set to be 100%. In the base demand scenario, implementing a CO_2 price of $30/tonne results in a large reduction of 66% of the total CO_2 emissions as coal is phased out. Further emissions reduction happens more gradually as the CO_2 price increase until 91% of the initial emissions are mitigated. The H_2 production in (b) is more reliant on SMR which results in a 16–55% increase in total emissions for CO_2 price less than $60/tonne. However, for CO_2 prices of $120/tonne or higher, H_2 is mostly produced from PEMEL (~80%) or SMR with CCS (~20%) resulting in a emissions increase of only 2% compared to (a).

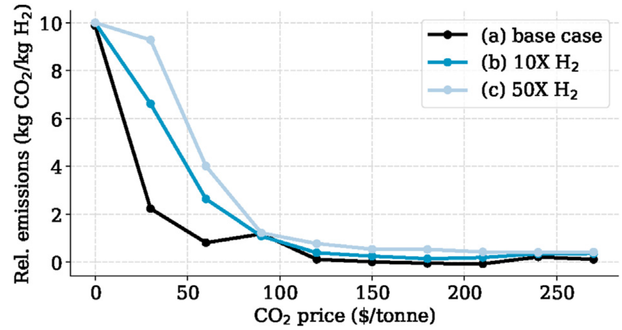

Fig. 8 – Relative CO_2 emissions from producing H_2.

Emissions increase to four times the base case at no CO_2 price for the highest H_2 demand in scenario (c). Producing these amounts of H_2 in Texas will result in significant increases in CO_2 emissions from the base case as it relies heavily on natural gas based H_2 production. For a CO_2 price of more than $90/tonne the emissions are reduced by a order of magnitude as CCS is implemented, and the emissions range between 22 and 58% of the reference value (100% mark) which is about twice the base case emissions for the same CO_2 prices.

We run the model for a scenario without H_2 production in order to quantify the emissions directly attributable to H_2 production. The emissions in the scenario with no H_2 production is subtracted from the total emissions in scenario (a)-(c) and divided by the total amount of H_2 produced in order to calculate the relative emissions (Fig. 8). For CO_2 prices of $0–90/tonne the relative emissions are reduced from 10 to 1.2 kg CO_2/kg H_2 as a large share of the H_2 production from CO_2 intensive SMR (10 kg CO_2/kg H_2) are phased out. H_2 production for CO_2 prices of $120/tonne or more is mostly based on PEMEL and SMR with CCS with a resulting carbon footprint ranging from (a) 0.11 to −0.07, (b) 0.14 to 0.39 and (c) 0.77 to 0.40 kg CO_2/kg H_2.

The relative CO_2 emissions for the base case is negligible or even negative for CO_2 prices ranging from $150–210/tonne. This is because flexible production of electrolytic H_2 displaces the need for flexible generation from CO_2-intensive natural

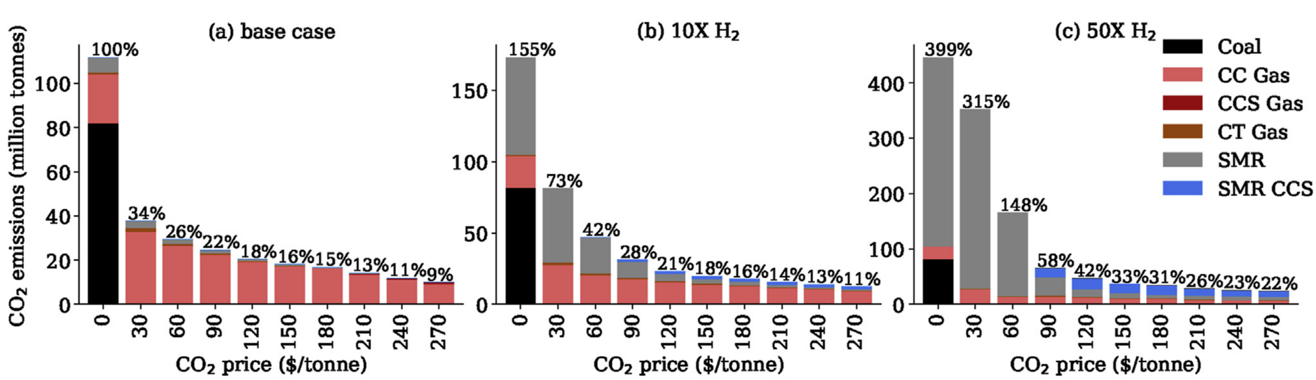

Fig. 7 – Total CO_2 emissions broken down by plant type. Base case with zero CO_2 price is set as reference at 100% for comparisons between the cases as the figures are of different scales.

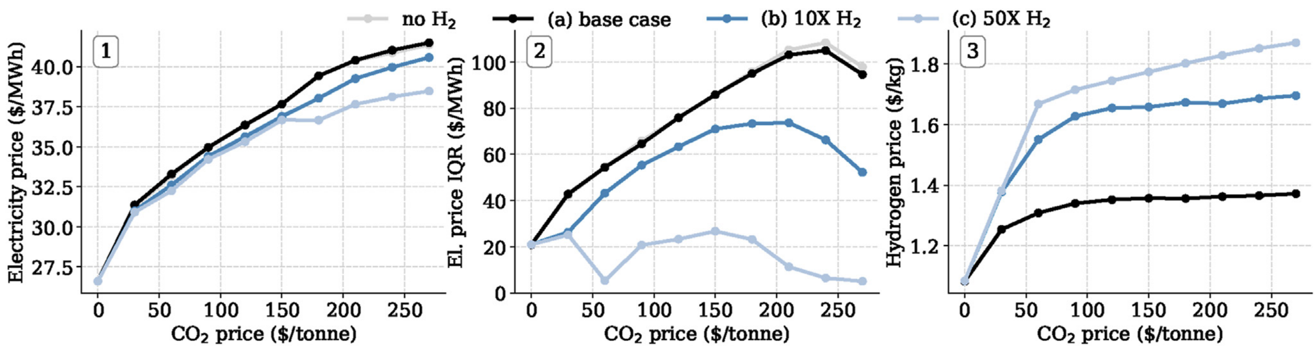

Fig. 9 – 1) average price cost of electricity production, 2) interquartile range (IQR) of the electricity price and 3) price of H_2 production, as a function of CO_2 price and H_2 demand. The IQR is the difference between the 25th and 75th quantile of the electricity price. The prices are weighted by the share of total electricity or H_2 produced at the different locations.

gas power plants, thus contributing to lower electricity sector emissions. The reduction in electricity sector emission is larger than the emissions caused by the H_2 production itself, resulting in lower total emissions for producing H_2. This is possible as most of the H_2 from natural gas include CCS for a CO_2 price of $150/tonne CO_2 and above, resulting in a low carbon footprint, while CCS for natural gas based electricity production does not emerge until $210/tonne.

Finally, note that the emissions impacts discussed here are only the emissions related to the production of H_2. Using this H_2 in an application such as H_2 vehicles would lead to further emission reductions from displacing petroleum-based fuels [80]. Using a fuel displacement of 2.46 gallons/kg H_2 [59] and 8.89 kg CO_2/gallon from the US Energy Information Administration (EIA), H_2 can displace around 21.9 kg CO_2/kg H_2 in light duty vehicles (not considering emissions from H_2 production). H_2 can also lead to significant emission reductions in the industrial sector, where replacing coke/coal in manufacturing of steel [81] is one of many applications.

Price of electricity and H_2 production

The marginal cost of electricity and H_2 production can be obtained from the optimization output as the dual values of the energy balances in H_2 and electricity nodes respectively, stated in Eq. (7). Below, we will refer to the systems marginal cost as the price, thus assuming perfect markets based on short-term marginal cost pricing which in theory minimize the average total cost of generation in the long run. In practice, these prices will deviate from real wholesale market prices as additional mechanisms (capacity markets, capacity payments, scarcity pricing etc.) are needed to address reliability and revenue sufficiency due to inherent wholesale market failures [82]. However, more realistic prices could be obtained by fixing the investments before obtaining the duals such that prices to only reflect short-term costs and not capital costs.

The average electricity price for the different scenarios of H_2 production is shown Fig. 9.1. The electricity price is similar for all the scenarios at low CO_2 prices as H_2 is mostly produced from SMR. The electricity price is lower for higher H_2 demands as the CO_2 price surpasses $30/tonne. The lower electricity price for higher H_2 demands can be explained by the mitigation of large amounts of battery and transmission capacity that otherwise would have been needed to integrate significant amounts of VRE electricity generation at high CO_2 prices. In addition, the flexible H_2 production enables phasing out of natural gas with less CCS and H_2 electricity generation that otherwise would increase the marginal cost of electricity production as seen for a CO_2 price of $180/tonne or higher.

Producing H_2 from electricity using flexible PEMEL has a smoothing effect on the electricity price as seen in Fig. 9.2, that shows the interquartile range (IQR) of the electricity price, i.e. the difference between the 25th and 75th quantile. The IQR of the electricity price increases with the CO_2 price and VRE deployment, this is balanced by investments in battery capacity that contains the spread in electricity prices. It is high in the base case but decreases significantly when more H_2 is produced in scenarios (b) and (c) due to the flexibility from hydrogen storage.

Similarly to the electricity price in Fig. 9.1, the H_2 price is shown in Fig. 9.3. These prices are in line with prices for H_2 production from wind power in Texas found by recent studies [59]. At zero CO_2 price the marginal H_2 production cost is similar for all the demand cases as H_2 production is exclusively from SMR. For a CO_2 price of $30/tonne the H_2 price is increased more for scenarios (b) and (c) as compared to the base case (a). Lower prices in (a) are achieved by producing higher amounts of H_2 from PEMEL at only 20% of the average electricity price, whereas (b) and (c) are more reliant on natural gas based H_2 with larger emissions and faces higher electricity prices for PEMEL. From a CO_2 price of $120/tonne the H_2 prices in case (a) and (b) are not significantly affected by the CO_2 price as 70–80% of the H_2 is produced from PEMEL and the rest is mostly produced from SMR with CCS at a low emission rate. For H_2 demand scenario (c) the H_2 price is increasing as up to 55% of the H_2 produced is based on SMR

Please cite this article as: Bødal EF et al., Decarbonization synergies from joint planning of electricity and hydrogen production: A Texas case study, International Journal of Hydrogen Energy, https://doi.org/10.1016/j.ijhydene.2020.09.127

with CCS, which have some emissions that drives the marginal cost with increasing CO_2 prices.

Discussion and conclusion

H_2 has the potential to be an important energy carrier that enables CO_2 emissions reductions, particularly in sectors and applications where direct electrification is too expensive or not feasible. Here, we implement a least-cost capacity expansion model with high temporal resolution for coordinated electricity and H_2 infrastructure planning that considers multiple technologies associated with generation and storage of both energy vectors. We specifically investigate the synergies between integration of VRE electricity production and flexible H_2 production by electrolysis (PEMEL) compared against H_2 production from SMR with or without CCS.

For a case study of Texas with pre-defined H_2 demand scenarios in 2050, we find that flexibility from producing H_2 enables larger shares of VRE to be integrated into the power system with less battery storage, as compared to the case with no H_2 demand. The simulated H_2 production by PEMEL correlate with wind power production and can help facilitate development of wind resources in the Texas pan handle (north-west) and southern part of the state. H_2 pipeline corridors are required across the demand scenarios to transport energy from west to east. The infrastructure outcomes are found to be sensitive to both the scale of H_2 demand (baseline, 10X, 50X) and CO_2 prices ($30–270/tonne). A share of VRE electricity generation of 94% is attainable with 1.3 GW of batteries and at a CO_2 of $60/tonne in the highest H_2 demand scenario while the same CO_2 price results in 78% VRE and 9.7 GW batteries in the lowest H_2 demand scenario. The maximum VRE share increase with the H_2 demand to a maximum of 86.4, 90.9 and 95.8% across the H_2 demand scenarios.

In the absence of CO_2 prices, SMR without CCS is the most cost-effective option for H_2 supply even with PEMEL capital costs that are roughly 50% lower than their costs in 2020. However, H_2 produced from electricity is strongly favored by increasing CO_2 prices and represents around half of the H_2 production at a relatively low CO_2 price of $30–60/tonne across the demand scenarios investigated here.

Flexible PEMEL operation complements VRE integration and displaces not only battery storage but also electricity production from natural gas and related emissions, by up to 5% in the lowest H_2 demand scenario and up to 53% in the highest demand scenario. Emissions attributable to serving H_2 demand generally increase with increasing H_2 demand for low CO_2 prices ($30–60/tonne), but are relatively small (less than 1.2 kg CO_2/kg H_2) beyond CO_2 prices of $90/tonne. Notably, for the baseline H_2 demand, the emissions attributable to H_2 demand are negative for CO_2 prices of $150–210/tonne. This suggests that H_2 production from electrolysis is a cost-effective solution to reduce carbon emissions, not only on the consumption side in for example fuel-cell vehicles, but also on the production side in the electric power system, as it enables higher levels of VRE in the system with less electricity from natural gas.

The integrated planning of H_2 and electricity infrastructure also reveals that deployment of CCS for H_2 production occurs at lower CO_2 prices ($90/tonne CO_2) than deployment of CCS for electricity generation ($180/tonne CO_2). Moreover, our estimate of CO_2 prices needed to make CCS-based power generation cost-effective are higher than those estimated by other studies [78], because we account for the impact of flexibility associated with new electricity demands (e.g. PEMEL operation) which reduce utilization of gas turbines. As a result, flexible H_2 production contributes to lowering and stabilizing the electricity price especially at CO_2 prices of $180/tonne or more as electricity generation from natural gas with CCS is reduced.

The marginal price of H_2 production does not see large changes for CO_2 prices above $90/tonne due to the synergies between flexible electrolysis and electricity generation from VRE. However, if the H_2 demand is very high, more of the H_2 will be produced by SMR with CCS for high CO_2 prices and the H_2 price is therefore somewhat sensitive to the CO_2 price.

The above framework can be adapted to study a broad range of technologies and sector-coupling issues. One area of future work would consider the role for other energy storage technologies such as compressed-air storage, electrochemical flow batteries or pumped hydro, which could compete with the flexible demand from the H_2 system. Another area of future work involves sector coupling with sectors needing heating and cooling end-use services where thermal storage could potentially be important. Incorporating temporal variability in H_2 demand can further increase the flexibility requirements provided by energy storage.

In our analysis, we only see small levels of re-conversion from H_2 to electricity at high CO_2 prices as it is expensive compared to CCS and the round-trip efficiency is low. Further sensitivity analysis on parameters such as carbon transport and storage cost, electrolyzer capital cost and natural gas prices could shed light on break-even points between cost of electricity generation from H_2 and natural gas with CCS.

Model improvements to be considered in future work include use of integer investment decisions for technologies with large plant sizes such as thermal power plants, transmission lines and SMR facilities. Representation of energy transport constraints for electricity and hydrogen can be enhanced by: a) employing DC power flow equations, b) model pipeline's ability to provide H_2 storage through line-packing and c) evaluating trade-off between truck and pipeline transport for H_2. These extensions will enable more accurate modeling of integrated H_2 and electricity infrastructure roll out.

To conclude, we point out that supporting adoption of H_2 in end-use applications and supplying that via electrolysis serves to benefit decarbonization and VRE integration in the power sector. This is contingent on electrolyzers to be able to effectively participate in electricity markets as we have envisioned here and regulators have a role in order create the right policies to make that happen.

Declaration of competing interest

The authors declare that they have no known competing financial interests or personal relationships that could have appeared to influence the work reported in this paper.

Acknowledgements

This publication is based on results from the research project Hyper, performed under the ENERGIX programme. The authors acknowledge the following parties for financial support: Equinor, Shell, Kawasaki Heavy Industries, Linde Kryotechnik, Mitsubishi Corporation, Nel Hydrogen and the Research Council of Norway (255107/E20) . D.S.M. contributed to this study while being supported by the Low-Carbon Energy Center on Electric Power Systems at the MIT Energy Initiative.

Appendix A. Illustrative example of Energy Balance

Here we give a illustrative example of the notation and energy balance used in the model. Consider the two nodes from Fig. 1, one electric and one H_2, which are connected by PEMEL and PEMFC. At the electric node, electricity is produced from wind and solar power, while H_2 is produced by SMR at the H_2 node.

The set of nodes is given by Eq. (A.1).

$$\mathcal{N} = \{1, 2\} \tag{A.1}$$

Node 1 is the electric node while node 2 is the H_2 node, thus the sets of production technologies at the nodes are shown in Eq. (A.2) and (A.3) respectively.

$$\mathcal{P}_1 = \{\text{Wind}, \text{Solar}, \text{PEMFC}\} \tag{A.2}$$

$$\mathcal{P}_2 = \{\text{SRM}, \text{PEMEL}\} \tag{A.3}$$

Similarly, we define the sets of storage technologies in Eq. (A.4) and (A.5).

$$\mathcal{S}_1 = \{\text{Battery}\} \tag{A.4}$$

$$\mathcal{S}_2 = \{\text{H}_2\ \text{Storage}\} \tag{A.5}$$

The conversion technologies producing at node n represents loads at another node given by the connectivity in set C_n. For our example, PEMFC producing electricity at node 1 consumes H_2 at node 2 as shown by Eq. (A.6). PEMEL producing H_2 at node 2 consumes electricity at node 1, shown by Eq. (A.7).

$$\mathcal{C}_1 = \{2\} \tag{A.6}$$

$$\mathcal{C}_2 = \{1\} \tag{A.7}$$

The conversion technology types representing the loads in C_n are given by the sets in Eq. (A.8) and (A.9).

$$\mathcal{F}_1 = \{\text{PEMEL}\} \tag{A.8}$$

$$\mathcal{F}_2 = \{\text{PEMFC}\} \tag{A.9}$$

The H_2 storage requires compression to 100 bar, this is represented as an auxiliary electric load at C_n by the set in Eq. (A.10).

$$\mathcal{A}_1 = \{\text{H}_2\ \text{Storage}\} \tag{A.10}$$

$$\mathcal{A}_2 = \{\} \tag{A.11}$$

From the sets we have defined and the generalized formulation of the energy balance in Eq. (7) the resulting energy balance for the electric node for time step t, is shown in (A.12).

$$\begin{aligned} & p_{t,\text{Wind},1} + p_{t,\text{Solar},1} + p_{t,\text{PEMFC},1} - p^{exp}_{t,1} + p^{imp}_{t,1} \\ & + (e^{out}_{t,\text{Battery},1} - e^{in}_{t,\text{Battery},1}) + r_{t,1} \\ & = D_{t,1} + F_{\text{PEMEL}} p_{t,\text{PEMEL},2} + A_{\text{H2S}} e^{in}_{t,\text{H2S},2} \end{aligned} \tag{A.12}$$

Similarly, the energy balance at the H_2 node in kg of H_2 is shown in Eq. (A.13).

$$\begin{aligned} & p_{t,\text{SMR},2} + p_{t,\text{PEMEL},2} - p^{exp}_{t,2} + p^{imp}_{t,2} \\ & + (e^{out}_{t,\text{H2S},2} - e^{in}_{t,\text{H2S},2}) + r_{t,2} \\ & = D_{t,2} + F_{\text{PEMFC}} p_{t,\text{PEMFC},1} \end{aligned} \tag{A.13}$$

Appendix B. Input Parameters

Table B.1 – Parameters used in the case study

Parameter	Value
Discount rate	6.6%
Retirement cost	10% of inv. cost
Natural gas price	$5.24/mmBtu
Rationing cost	$10 000/MWh
	$10 000/kg H$_2$
Carbon storage and transport cost	$11/tonne

Table B.2 – Installed capacity in 2019 adopted from the NEEDS model [55].

Bus	CC Gas [MW]	CT Gas [MW]	Nuclear [MW]	Wind [MW]	Solar [MW]	Coal [MW]	Biomass [MW]
1	6598	5621	2400	2168	24		
2				3999	340		
3		1540		5842		2085	
4	9729	8191					146
5				1051	141		
6	2850	3190		7913	873		
7	1943	1008			5	5744	
8	3098	2064		543	96	2371	
9	4072	1843		1680	52	940	
	4118	2490	2560			2507	
11	4854	1726				4187	5
12	2949	618		4849			18
13				998	905		
Sum	40,211	28,291	4,960	29,043	2,436	17,834	169

Table B.3 – Technology costs for 2050 from NREL ATB technology baseline [65]. Fuel units (f.u.) are mmBtu for natural gas and kg for hydrogen.

Type	Inv. cost ($/kW)	Fixed cost ($/kW-year)	Var. cost ($/MWh)	Fuel (f.u./ MWh)	Emission (kg/MWh)	CCS rate (kg/MWh)	Size (MW)	Min. Gen. (MW)	Ramp Rate (%/h)	Lifetime (years)
Wind	1011	33	0	0	0	0	100	0	1	30
Solar	683	8	0	0	0	0	150	0	1	30
CT Gas	800	12	7	9.08	481.6	0	240	0	1	55
CC Gas	800	11	3	6.28	333	0	1100	0	0.252	55
CCS Gas	1730	34	7	7.49	39.8	358.2	340	0	0.252	55
Coal	3640	33	24.1	0	834.7	0	650	260	0.1584	75
CCS Coal	5240	80	30.2	0	88.4	795.6	650	325	0.1584	75
Nuclear	5530	101	9.6	0	0	0	2200	2200	0.156	60
Biomass	3490	112	46.9	0	0	0	85	34	0.32	45
CC H2	900	13	2.8	5.69	0	0	1100	0	0.252	25
CT H2	600	6	8.8	8.54	0	0	240	0	1	25
PEMFC	1090	0	8.9	6.7	0	0	50	0	1	10

Table B.4 – Technology costs in 2040 are obtained from the NREL centralized H_2 production case studies for electrolysis [9] and from a IEA GHG technical report on SMR with CCS [64]. Electricity for the SMR and CO_2 capture processes are generated by on-site gas turbines [64].

Type	Inv. cost ($/(kg/h))	Fixed cost ($/(kg/h))	Var. cost ($/kg)	Fuel (mmBtu/ kg)	Electricity (MWh/kg)	Emission (kg CO_2/ kg H_2)	CCS rate (kg CO_2/ kg H_2)	Size (kg/h)	Min. Gen. (kg/h)	Ramp Rate (%/h)	Lifetime (years)
SMR	33800	0	0	0.146	0	10	0	9170	8250	0.1	25
SMR CCS	73480	0	0	0.16	0	0.99	9.01	9170	8250	0.1	25
PEMEL	27310	1915	0	0	51.3	0	0	2000	0	1	40

Table B.5 – Technology costs for storage technologies [9,67,70,71]. Units for the different storage technologies are specified by p.u. and e.u. for power and energy respectively.

Type	p.u.	e.u.	Inv. power ($/pu)	Inv. energy ($/eu)	Fix power ($/pu-yr)	Fix energy ($/eu-yr)	Ramp (%/h)	Eff. In/ Out	Aux power (kWh/eu)	Life (years)
Battery storage	kW	kWh	273	84	15.19	0	1	0.92	0	15
Hydrogen storage	kg/h	Kg	1540	516	46	2	1	1	1.284	40

Please cite this article as: Bødal EF et al., Decarbonization synergies from joint planning of electricity and hydrogen production: A Texas case study, International Journal of Hydrogen Energy, https://doi.org/10.1016/j.ijhydene.2020.09.127

Table B.6 – H_2 demand per node based on high case for adoption of fuel cell vehicles [kg/day] [58].

Bus	1	2	3	4	5	6	7	8	9	10	11	13
H2 demand	764 200	300	3210	334 920	1550	13 240	2390	200 570	190 450	333 950	4250	20 350

REFERENCES

[1] International Energy Agency. World energy outlook 2018. Tech. Rep.. 2018. https://doi.org/10.1787/weo-2018-2-en. 0

[2] Ruhnau O, Bannik S, Otten S, Praktiknjo A, Robinius M. Direct or indirect electrification? A review of heat generation and road transport decarbonisation scenarios for Germany 2050. Energy 2019;166:989–99. https://doi.org/10.1016/j.energy.2018.10.114.

[3] Robinius M, Linßen J, Grube T, Reuß M, Stenzel P, Syranidis K, Kuckertz P, Stolten D. Comparative analysis of infrastructures: hydrogen fueling and electric charging of vehicles. Tech. Rep. January. Forschungszentrums Jülich; 2018.

[4] Tlili O, Mansilla C, Frimat D, Perez Y. Hydrogen market penetration feasibility assessment: mobility and natural gas markets in the US, Europe, China and Japan. Int J Hydrogen Energy 2019;44(31):16048–68. https://doi.org/10.1016/j.ijhydene.2019.04.226.

[5] Horvath S, Fasihi M, Breyer C. Techno-economic analysis of a decarbonized shipping sector: technology suggestions for a fleet in 2030 and 2040. Energy Convers Manag 2018;164(November 2017):230–41. https://doi.org/10.1016/j.enconman.2018.02.098.

[6] García-Olivares A, Solé J, Osychenko O. Transportation in a 100% renewable energy system. Energy Convers Manag 2018;158(August 2017):266–85. https://doi.org/10.1016/j.enconman.2017.12.053.

[7] Schemme S, Breuer JL, Köller M, Meschede S, Walman F, Samsun RC, Peters R, Stolten D. H2-based synthetic fuels: a techno-economic comparison of alcohol, ether and hydrocarbon production. Int J Hydrogen Energy 2020;45(8):5395–414. https://doi.org/10.1016/j.ijhydene.2019.05.028.

[8] IEA - International Energy Agency. The Future of Hydrogen – seizing today's opportunities. Tech. rep. 2019;2019:1–203. URL, https://www.iea.org/reports/the-future-of-hydrogen.

[9] National Renewable Energy Laboratory. H2A: hydrogen analysis production case studies — hydrogen and fuel cells. NREL; 2019. URL, https://www.nrel.gov/hydrogen/h2a-production-case-studies.html.

[10] Saba SM, Müller M, Robinius M, Stolten D. The investment costs of electrolysis – a comparison of cost studies from the past 30 years. Int J Hydrogen Energy 2018;43(3):1209–23. https://doi.org/10.1016/J.IJHYDENE.2017.11.115.

[11] Schmidt O, Gambhir A, Staffell I, Hawkes A, Nelson J, Few S. Future cost and performance of water electrolysis: an expert elicitation study. Int J Hydrogen Energy 2017;42(52):30470–92. https://doi.org/10.1016/j.ijhydene.2017.10.045.

[12] Proost J. Critical assessment of the production scale required for fossil parity of green electrolytic hydrogen. Int J Hydrogen Energy 2020;2050. https://doi.org/10.1016/j.ijhydene.2020.04.259 (xxxx).

[13] Levene JI, Mann MK, Margolis RM, Milbrandt A. An analysis of hydrogen production from renewable electricity sources. Sol Energy 2007;81(6):773–80. https://doi.org/10.1016/J.SOLENER.2006.10.005.

[14] Korpås M, Greiner CJ. Opportunities for hydrogen production in connection with wind power in weak grids. Renew Energy 2008;33(6):1199–208. https://doi.org/10.1016/j.renene.2007.06.010.

[15] Beccali M, Brunone S, Finocchiaro P, Galletto JM. Method for size optimisation of large wind-hydrogen systems with high penetration on power grids. Appl Energy 2013;102:534–44. https://doi.org/10.1016/j.apenergy.2012.08.037.

[16] Lund PD, Lindgren J, Mikkola J, Salpakari J. Review of energy system flexibility measures to enable high levels of variable renewable electricity. Renew Sustain Energy Rev 2015;45:785–807. https://doi.org/10.1016/J.RSER.2015.01.057.

[17] Lyseng B, Niet T, English J, Keller V, Palmer-Wilson K, Robertson B, Rowe A, Wild P. System-level power-to-gas energy storage for high penetrations of variable renewables. Int J Hydrogen Energy 2018;43(4):1966–79. https://doi.org/10.1016/J.IJHYDENE.2017.11.162.

[18] McPherson M, Johnson N, Strubegger M. The role of electricity storage and hydrogen technologies in enabling global low-carbon energy transitions. Appl Energy 2018;216:649–61. https://doi.org/10.1016/j.apenergy.2018.02.110.

[19] Glenk G, Reichelstein S. Economics of converting renewable power to hydrogen. Nature Energy 2019;4(3):216–22. https://doi.org/10.1038/s41560-019-0326-1.

[20] Proost J. State-of-the art CAPEX data for water electrolysers, and their impact on renewable hydrogen price settings. Int J Hydrogen Energy 2019;44(9):4406–13. https://doi.org/10.1016/j.ijhydene.2018.07.164.

[21] Wang D, Muratori M, Eichman J, Wei M, Saxena S, Zhang C. Quantifying the flexibility of hydrogen production systems to support large-scale renewable energy integration. J Power Sources 2018;399(August):383–91. https://doi.org/10.1016/j.jpowsour.2018.07.101.

[22] Bødal EF, Korpås M. Regional effects of hydrogen production in congested transmission grids with wind and hydro power. In: 14th International Conference on the European Energy Market - EEM. IEEE; 2017. p. 1–6. https://doi.org/10.1109/EEM.2017.7982013.

[23] Greiner CJ. Doctoral thesis: sizing and operation of wind-hydrogen energy systems. Ph.D. thesis. NTNU; 2010.

[24] Botterud A, Yildiz B, Conzelmann G, Petri MC. Nuclear hydrogen: an assessment of product flexibility and market viability. Energy Pol 2008;36(10):3961–73. https://doi.org/10.1016/j.enpol.2008.07.007.

[25] Greiner CJ, Korpas M, Gjengedal T. Dimensioning and operating wind-hydrogen plants in power markets. In: 12th WSEAS International Conference on CIRCUITS; 2008. p. 405–14.

[26] Greiner CJ, Korpas M, Gjengedal T. A model for techno-economic optimization of wind power combined with hydrogen production in weak grids. EPE Journal 2009;19(2):52–9. https://doi.org/10.1080/09398368.2009.11463717.

[27] Peterson D, Vickers J, DeSantis D. Hydrogen production cost from PEM electrolysis - 2019. Tech. rep. Department of Energy; 2020. URL, https://www.hydrogen.energy.gov/pdfs/19009_h2_production_cost_pem_electrolysis_2019.pdf.

[28] Korpås M. Distributed energy systems with wind power and energy storage, vol. 183; 2004. p. 1–80.

[29] Kopp M, Coleman D, Stiller C, Scheffer K, Aichinger J, Scheppat B. Energiepark Mainz: technical and economic analysis of the worldwide largest Power-to-Gas plant with

PEM electrolysis. Int J Hydrogen Energy 2017;42(19). https://doi.org/10.1016/j.ijhydene.2016.12.145.
[30] Bødal EF, Korpås M. Value of hydro power flexibility for hydrogen production in constrained transmission grids. Int J Hydrogen Energy 2020;45(2):1255–66. https://doi.org/10.1016/j.ijhydene.2019.05.037.
[31] Alshehri F, Suárez VG, Rueda Torres JL, Perilla A, van der Meijden MA. Modelling and evaluation of PEM hydrogen technologies for frequency ancillary services in future multi-energy sustainable power systems. Heliyon 2019;5(4). https://doi.org/10.1016/j.heliyon.2019.e01396. e01396.
[32] Go RS, Munoz FD, Watson J-P. Assessing the economic value of co-optimized grid-scale energy storage investments in supporting high renewable portfolio standards. Appl Energy 2016;183:902–13. https://doi.org/10.1016/J.APENERGY.2016.08.134.
[33] Mallapragada DS, Sepulveda NA, Jenkins JD. Long-run system value of battery energy storage in future grids with increasing wind and solar generation. Appl Energy 2020;275(February):115390. https://doi.org/10.1016/j.apenergy.2020.115390.
[34] Colbertaldo P, Agustin SB, Campanari S, Brouwer J. Impact of hydrogen energy storage on California electric power system: towards 100% renewable electricity. Int J Hydrogen Energy 2019;44(19):9558–76. https://doi.org/10.1016/J.IJHYDENE.2018.11.062.
[35] Liu H, Brown T, Andresen GB, Schlachtberger DP, Greiner M. The role of hydro power, storage and transmission in the decarbonization of the Chinese power system. Appl Energy 2019;239(November 2018):1308–21. https://doi.org/10.1016/j.apenergy.2019.02.009.
[36] Welder L, Ryberg D, Kotzur L, Grube T, Robinius M, Stolten D. Spatio-temporal optimization of a future energy system for power-to-hydrogen applications in Germany. Energy 2018;158:1130–49. https://doi.org/10.1016/j.energy.2018.05.059.
[37] Welder L, Stenzel P, Ebersbach N, Markewitz P, Robinius M, Emonts B, Stolten D. Design and evaluation of hydrogen electricity reconversion pathways in national energy systems using spatially and temporally resolved energy system optimization. Int J Hydrogen Energy 2019;44(19):9594–607. https://doi.org/10.1016/J.IJHYDENE.2018.11.194.
[38] Emonts B, Reuß M, Stenzel P, Welder L, Knicker F, Grube T, Görner K, Robinius M, Stolten D. Flexible sector coupling with hydrogen: a climate-friendly fuel supply for road transport. Int J Hydrogen Energy 2019;44(26):12918–30. https://doi.org/10.1016/j.ijhydene.2019.03.183.
[39] Samsatli S, Staffell I, Samsatli NJ. Optimal design and operation of integrated wind-hydrogen-electricity networks for decarbonising the domestic transport sector in Great Britain. Int J Hydrogen Energy 2016;41(1):447–75. https://doi.org/10.1016/j.ijhydene.2015.10.032.
[40] Koltsaklis NE, Dagoumas AS. State-of-the-art generation expansion planning: a review. Appl Energy 2018;230:563–89. https://doi.org/10.1016/J.APENERGY.2018.08.087.
[41] Victoria M, Zhu K, Brown T, Andresen GB, Greiner M. The role of storage technologies throughout the decarbonisation of the sector-coupled European energy system. Energy Convers Manag 2019;201:111977. https://doi.org/10.1016/j.enconman.2019.111977.
[42] Blanco H, Nijs W, Ruf J, Faaij A. Potential for hydrogen and Power-to-Liquid in a low-carbon EU energy system using cost optimization. Appl Energy 2018;232:617–39. https://doi.org/10.1016/j.apenergy.2018.09.216.
[43] Pan G, Gu W, Qiu H, Lu Y, Zhou S, Wu Z. Bi-level mixed-integer planning for electricity-hydrogen integrated energy system considering levelized cost of hydrogen. Appl Energy 2020;270(May):115176. https://doi.org/10.1016/j.apenergy.2020.115176.
[44] Kanellopoulos K, Blanco H. The potential role of H2 production in a sustainable future power system - an analysis with METIS of a decarbonised system powered by renewables in 2050. Tech. rep. European Commission; 2019. https://doi.org/10.2760/540707.
[45] Lux B, Pfluger B. A supply curve of electricity-based hydrogen in a decarbonized European energy system in 2050. Appl Energy 2020;269(April):115011. https://doi.org/10.1016/j.apenergy.2020.115011.
[46] Cloete S, Hirth L. Flexible power and hydrogen production: finding synergy between CCS and variable renewables. Energy 2020;192:116671. https://doi.org/10.1016/j.energy.2019.116671.
[47] Lim JY, How BS, Rhee G, Hwangbo S, Yoo CK. Transitioning of localized renewable energy system towards sustainable hydrogen development planning: P-graph approach. Appl Energy 2020;263(November 2019):114635. https://doi.org/10.1016/j.apenergy.2020.114635.
[48] You C, Kwon H, Kim J. Economic, environmental, and social impacts of the hydrogen supply system combining wind power and natural gas. Int J Hydrogen Energy 2020. https://doi.org/10.1016/j.ijhydene.2020.06.095.
[49] Palmintier BS, Webster MD. Heterogeneous unit clustering for efficient operational flexibility modeling. IEEE Trans Power Syst 2014;29(3):1089–98. https://doi.org/10.1109/TPWRS.2013.2293127.
[50] Palmintier BS. Incorporating operational flexibility into electric generation planning - impacts and methods for system design and policy analysis. Ph.D. thesis. Massachusetts Institute of Technology; 2013. URL, https://dspace.mit.edu/handle/1721.1/79147.
[51] Hart WE, Watson JP, Woodruff DL. Pyomo: modeling and solving mathematical programs in Python. Mathematical Programming Computation 2011;3(3):219–60. https://doi.org/10.1007/s12532-011-0026-8.
[52] Hart WE, Laird CD, Watson J-P, Woodruff DL, Hackebeil GA, Nicholson BL, Siirola JD. Optimization modeling in Python - springer optimization and its applications, vol. 67. Springer Nature; 2017. https://doi.org/10.1007/978-3-319-58821-6.
[53] Du P, Baldick R, Tuohy A. Integration of large-scale renewable energy into bulk power systems - from planning to operation, power electronics and power systems. Cham: Springer International Publishing; 2017. https://doi.org/10.1007/978-3-319-55581-2.
[54] Majidi-Qadikolai M, Baldick R. Stochastic transmission capacity expansion planning with special scenario selection for integrating $n-1$ contingency analysis. IEEE Trans Power Syst 2016;31(6):4901–12. https://doi.org/10.1109/TPWRS.2016.2523998.
[55] United States Environmental Protection Agency. Documentation for national electric energy data system (NEEDS) v.5.13. URL, https://www.epa.gov/airmarkets/documentation-national-electric-energy-data-system-needs-v513; 2019.
[56] U.S. EIA. Annual energy outlook 2019 with projections to 2050, annual energy outlook 2019 with projections to 2050, vol. 44; 2019. p. 1–64 (8) DOE/EIA-0383(2012) U.S.
[57] Mann N, Tsai C-H, Gürcan G, Schneider E, Cuevas P, Dyer J, Butler J, Zhang T, Baldick R, Deetjen T, Morneau R. The full cost of electricity (FCe-) capacity expansion and dispatch modeling: model documentation and results for ERCOT scenarios. Tech. rep. University of Texas at Austin; 2017.
[58] Melaina M, Bush B, Muratori M, Zuboy J, Ellis S. National hydrogen scenarios: how many stations, where, and when?. Tech. Rep. October, Prepared by the National Renewable

Please cite this article as: Bødal EF et al., Decarbonization synergies from joint planning of electricity and hydrogen production: A Texas case study, International Journal of Hydrogen Energy, https://doi.org/10.1016/j.ijhydene.2020.09.127

Energy Laboratory for the H2 USA Locations Roadmap Working Group; 2017.
[59] Nagasawa K, Davidson FT, Lloyd AC, Webber ME. Impacts of renewable hydrogen production from wind energy in electricity markets on potential hydrogen demand for light-duty vehicles. Appl Energy 2019;235(June 2018):1001–16. https://doi.org/10.1016/j.apenergy.2018.10.067.
[60] Elgowainy A. Hydrogen demand analysis for H2 @ scale. URL, https://www.hydrogen.energy.gov/pdfs/review19/sa172_elgowainy_2019_o.pdf; 2019.
[61] Ruth M. H2 @ scale: hydrogen integrating energy systems. URL, https://www.nrel.gov/docs/fy20osti/75422.pdf; 2019.
[62] Parkinson B, Balcombe P, Speirs JF, Hawkes AD, Hellgardt K. Levelized cost of CO 2 mitigation from hydrogen production routes. Energy Environ Sci 2019;12(1):19–40. https://doi.org/10.1039/c8ee02079e.
[63] Khojasteh Salkuyeh Y, Saville BA, MacLean HL. Techno-economic analysis and life cycle assessment of hydrogen production from natural gas using current and emerging technologies. Int J Hydrogen Energy 2017. https://doi.org/10.1016/j.ijhydene.2017.05.219.
[64] IEA. Techno - economic evaluation of SMR based standalone (merchant) hydrogen plant with CCS. Tech. Rep. February. Paris, France: IEA; 2017. URL, http://ieaghg.org/exco_docs/2017-02.pdf.
[65] National Renewable Energy Laboratory (NREL). Annual technology baseline: electricity (2019). 2019. URL, https://atb.nrel.gov/.
[66] Grant T, Morgan D, Gerdes K. Quality guidelines for energy system studies: carbon dioxide transport and storage costs in NETL studies. Tech. Rep. August. National Energy Technology Laboratory; 2019.
[67] van Leeuwen C, Zauner A. Innovative large-scale energy storage technologies and Power-to-Gas concepts after optimisation. Report on the costs involved with PtG technologies and their potentials across the EU, Tech. Rep. University of Groningen; 2018. URL, https://www.storeandgo.info/publications/deliverables/.
[68] Cooley G, Allen A. Interim results presentation 2019. 2019. URL, https://www.itm-power.com/images/Investors/PresentationsAndResearch/Interim-Results-presentation_18.pdf.
[69] André J, Auray S, De Wolf D, Memmah MM, Simonnet A. Time development of new hydrogen transmission pipeline networks for France. Int J Hydrogen Energy 2014;39(20):10323–37. https://doi.org/10.1016/j.ijhydene.2014.04.190.
[70] Ahluwalia RK, Contact P, Peng J-k, Manager DOE, Randolph K. System Analysis of physical and materials-based hydrogen storage. Tech. rep. DOE Hydrogen and Fuel Cells Program; 2018. URL, https://www.hydrogen.energy.gov/pdfs/progress19/h2f_st001_ahluwalia_2019.pdf.
[71] Ahluwalia RK, Hua TQ, Peng J-K, Roh HS. System level analysis of hydrogen storage options. Project ID: ST001. 2019. URL, https://www.hydrogen.energy.gov/pdfs/review19/st001_ahluwalia_2019_o.pdf.
[72] Caglayan DG, Weber N, Heinrichs HU, Linßen J, Robinius M, Kukla PA, Stolten D. Technical potential of salt caverns for hydrogen storage in Europe. Int J Hydrogen Energy 2020;45(11):6793–805. https://doi.org/10.1016/j.ijhydene.2019.12.161.
[73] Tarkowski R. Underground hydrogen storage: characteristics and prospects. 2019. https://doi.org/10.1016/j.rser.2019.01.051. 5.
[74] Andrade J, Baldick R. Estimation of transmission costs for new generation. Tech. rep. University of Texas at Austin; 2017.
[75] Lee N, Flores-Espino F, Hurlbut D. Renewable energy zones (REZ) transmission planning process: a Guidebook for practitioners. 2017. URL, https://www.nrel.gov/docs/fy17osti/69043.pdf.
[76] Lasher W. The competitive renewable energy zones process. Ercot; 2014.
[77] United States Environmental Protection Agency (EPA). Social cost of carbon. Tech. Rep. December. US EPA; 2016. URL, https://www.epa.gov/sites/production/files/2016-12/documents/social_cost_of_carbon_fact_sheet.pdf.
[78] Mathieu P. The IPCC special report on carbon dioxide capture and storage. 2006.
[79] European Comission. A hydrogen strategy for a climate neutral europe. 2020.
[80] Andress D, Nguyen TD, Das S. Reducing GHG emissions in the United States' transportation sector. 2011. https://doi.org/10.1016/j.esd.2011.03.002.
[81] Vogl V, Åhman M, Nilsson LJ. Assessment of hydrogen direct reduction for fossil-free steelmaking. J Clean Prod 2018;203:736–45. https://doi.org/10.1016/j.jclepro.2018.08.279.
[82] Milligan M, Frew B, Clark K, Bloom A. Marginal cost pricing in a world without perfect competition: implications for electricity markets with high shares of low marginal cost resources. Tech. Rep. December. NREL; 2017.

Acronyms

CCS: carbon capture and storage
EIA: US Energy Information Administration
EPA: US Environmental Protection Agency
ERCOT: Electric Reliability Council of Texas
GHG: greenhouse gas
LCOE: levelized cost of energy
LHV: lower heating value
LP: linear programming
NREL: National Renewable Energy Laboratory
PEMEL: proton exchange membrane electrolysis
PEMFC: proton exchange membrane fuel cell
SMR: steam-methane reforming
VRE: variable renewable energy

Please cite this article as: Bødal EF et al., Decarbonization synergies from joint planning of electricity and hydrogen production: A Texas case study, International Journal of Hydrogen Energy, https://doi.org/10.1016/j.ijhydene.2020.09.127